Space-Time Accurate Finite-State Dynamic Inflow Modeling for Aeromechanics of Rotorcraft

Felice Cardito, Riccardo Gori, Jacopo Serafini,
Giovanni Bernardini,, Massimo Gennaretti*

Department of Engineering, Roma Tre University, Via della Vasca Navale, 79, 00146, Rome, Italy

Abstract

Wake inflow modeling is a crucial issue in the development of efficient and high-fidelity simulation tools for rotorcraft flight dynamics and aeroelasticity. This paper proposes a space-time accurate, finite-state, dynamic wake inflow modeling suitable for conventional and innovative rotor configurations, based on simulations provided by high-fidelity aerodynamic solvers. It relates the coefficients of a rotor-disc, radial-azimuthal wake inflow distribution to the rotor kinematic variables, and is capable to take into account the intrinsic periodicity of aerodynamic responses of rotors in steady forward flight. The proposed inflow modeling consists of a three-step process: (i) numerical evaluation of wake inflow due to perturbations of rotor kinematic variables, (ii) determination of transfer functions of multi-harmonic components of a suitable set of inflow coordinates, followed by (iii) their rational approximation and transformation into time domain to derive the differential operators governing multi-harmonic dynamics. The numerical investigation concerns the derivation of finite-state inflow models for single and coaxial rotors, through application of an aerodynamic boundary-element-method solver for potential flows. These are successfully validated by comparison with inflows directly calculated by the aerodynamic tool for arbitrary rotor perturbations.

*Corresponding author.
Email address: massimo.gennaretti@uniroma3.it (Massimo Gennaretti)

1. Introduction

A crucial role in the dynamic behavior of rotorcraft is played by rotor blade aerodynamic loads which, in turn, are strongly affected by the corresponding wake inflow generated on the rotor disc. The introduction of dynamic inflow models has been a milestone in the development of helicopter simulation tools, in that it allows the efficient estimation of blade effective angle of attack.

Although available aerodynamic solvers based on three-dimensional, unsteady formulations can provide accurate predictions of blade loads, their computational cost is still too high for typical design purposes, thus making the sectional-aerodynamics/wake-inflow combination a still convenient solution process for aeroelastic, flight dynamics and flight control system analyses. On the other hand, finite-state, dynamic inflow modeling is an effective approach to include the wake unsteady effects in rotorcraft simulation tools, especially when stability analyses are requested. Most of the available finite-state inflow models are based on closed-form, acceleration-potential aerodynamic solutions over an actuator disk. Widely-used examples are the Pitt-Peters [1], [2] and the Peters-He [3] models, along with their extended versions which take into account wake distortion effects (see, for instance, [4, 5, 6]). Based on simplifying assumptions for the flow field solution, they are computationally very efficient. The Pitt-Peters model is suitable for low-frequency flight dynamics simulations, whereas the Peters-He one, with the introduction of more accurate approximation forms of azimuthal and radial inflow distributions, is applicable also to aeroelastic problems.

Recently, great attention has been paid to the development of tools for non-conventional helicopter configurations. Indeed, the models mentioned above can be effectively used for analyses of single-rotor helicopters, but are unsuitable for more complex configurations like, for instance, coaxial contra-rotating rotors. Through application of enhanced momentum theory, state-space dynamic models of coaxial rotor wake inflow capable to take into account the mutual aerodynamic interference between the rotors have been developed as extensions of the Peters-He model [7, 8, 9]. However, the low accuracy of the aerodynamic models they are based on, make them unable to capture important features of the complex aerodynamic field related, for instance, to the strong interac-

tions among wake vorticity and rotor blades. Thus, corrections to these models relying on CFD simulations have been recently proposed [10]. Note that, in this context, corrections based on experimental measurements cannot be applied since the extraction from the velocity field of the component directly induced by the wake vorticity is not feasible. Indeed, validations of rotor aerodynamic simulation tools usually concern the total inflow and/or indirect outcomes like, for instance, blade loads (see, for instance, [3, 11, 12]).

The objective of this paper is to present a methodology to extract radial/azimuth-accurate, finite-state, linear time-periodic (LTP) rotor inflow dynamic models from simulations provided by high-fidelity aerodynamics solvers. Based on the combination of linear time-invariant (LTI) dynamics of multi-harmonic components, this modeling approach relates wake inflow to rotor kinematic variables perturbations. Differently from models based on analytical solutions, complex aerodynamic phenomena like rotor/fuselage or rotor/rotor interactional effects, or those arising in non-conventional rotorcraft configurations or flight conditions are taken into account, if suitably predicted by the numerical simulation. The proposed technique can be considered as a development of the LTI, finite-state inflow modeling suitable for helicopter flight dynamics applications introduced by the authors in [13, 14], extended to coaxial rotor configurations in [15, 16], and closely related to the work presented in [17, 18]. The model parameters introduced are such to describe with arbitrary accuracy radial and azimuthal inflow distributions. They are identified by an innovative multi-step technique, similar to that proposed in [13, 14], but capable of taking into account the time-periodic characteristics of the aerodynamic operators typical of steady flight of advancing single rotors and coaxial rotor systems. First, the relationships between perturbations of kinematic variables and perturbations of wake inflow on rotor blades are expressed in terms of transfer functions determined by analysis of the harmonic content of suited time-marching aerodynamic responses. Then a rational-form approximation algorithm is applied for their finite-state representation [19, 20]. The final model consists of multi-harmonic components combination, with components dynamics governed by ordinary differential equations forced by rotor kinematics.

In order to apply and validate the proposed space-time accurate multi-harmonic dy-

namic inflow modeling technique, the wake inflow responses are evaluated by a Boundary Element Method (BEM) free-wake solver for potential-flows [21]. It is capable of simulating the aerodynamic interference effects in multi-body configurations (like coaxial rotors or rotor-fuselage systems), as well as severe blade-vortex interactions. Specifically, the numerical applications are illustrated and discussed in Section 3, and concern wake inflow modeling of both single-rotor and coaxial-rotor configurations in forward flight.

2. Space-Time Accurate Multi-Harmonic Finite-State Inflow Modeling

The main steps of the proposed technique for the extraction of finite-state, wake inflow models from arbitrary high-fidelity aerodynamic simulations are: i) definition of suited approximation forms of inflow radial and azimuthal distributions; ii) decomposition of the corresponding time-dependent coefficients (inflow coordinates) into multi-harmonic dynamic components, and identification (extraction) of the transfer functions (LTI representations) relating them to rotor kinematic perturbations, from a suitable set of time responses predicted by the aerodynamic solver; iii) rational approximation of the transfer functions and determination of the multi-harmonic components LTI, finite-state, dynamic models; iv) definition of the final LTP, finite-state, dynamic inflow model as combination of the identified LTI operators for multi-harmonic dynamics.

In the following, these steps are described in detail for the case of a single rotor, with the extension to coaxial rotors outlined in Section 2.5.

2.1. Inflow Radial-Azimuthal Representation

In order to represent the complex wake inflow field with a level of accuracy suitable for flight mechanics and aeroelastic applications, it is expressed in a non-rotating frame in terms of spanwise-varying multiblade variables.

Indeed, introducing the hub-fixed polar coordinate system (r, ψ) over the rotor disc, for a four-bladed rotor, the wake inflow perturbation, ν, on the i-th blade at the azimuth position ψ_i is expressed using the following Coleman transformation form as an

extension of those considered in [1, 3, 14]

$$\nu(r,\psi_i,t) = \nu_0(r,t) + \nu_c(r,t)\,\cos\psi_i + \nu_s(r,t)\,\sin\psi_i + \nu_{N/2}(r,t)\,(-1)^i \qquad (1)$$

where ν_0, ν_c, ν_s and $\nu_{N/2}$ are, respectively, instantaneous collective, cosine and sine cyclic and differential inflow coefficients at a given radial position, r. For ν_i denoting the wake inflow perturbation evaluated by the high-fidelity aerodynamic tool on the i-th rotor blade, the application of the separation variables technique and the introduction of suitable sets of linearly independent radial basis functions, $\phi_j^\alpha(r)$, yield the following expressions for the wake inflow coefficients

$$\begin{aligned}
\nu_0(r,t) &= \frac{1}{N_b}\sum_{i=1}^{N_b}\nu_i(r,t) = \sum_{j=1}^{N_0^r}\lambda_j^0(t)\;\phi_j^0(r)\\
\nu_c(r,t) &= \frac{2}{N_b}\sum_{i=1}^{N_b}\nu_i(r,t)\cos\psi_i = \sum_{j=1}^{N_c^r}\lambda_j^c(t)\;\phi_j^c(r)\\
\nu_s(r,t) &= \frac{2}{N_b}\sum_{i=1}^{N_b}\nu_i(r,t)\sin\psi_i = \sum_{j=1}^{N_s^r}\lambda_j^s(t)\;\phi_j^s(r)\\
\nu_{N/2}(r,t) &= \frac{1}{N_b}\sum_{i=1}^{N_b}\nu_i(r,t)\,(-1)^i = \sum_{j=1}^{N_{N/2}^r}\lambda_j^{N/2}(t)\;\phi_j^{N/2}(r)
\end{aligned} \qquad (2)$$

where N_b denotes the number of rotor blades, N_α^r is the number of functions used to define the α-coefficient radial distribution, λ_j^α represent the components of the inflow α-coefficient on the basis functions ϕ_j^α (here called inflow coordinates). The differential component ($\alpha = N/2$) appears only for rotors with an even number of blades, whereas higher-harmonic cyclic components ($\nu_{2c}, \nu_{2s}, \ldots$) are included when $N_b > 4$. As it will be shown later, the introduction, when required, of the differential inflow coefficient assures the capability of the expression in Eq. 1 of capturing the entire inflow spectrum.

It is worth noting that, neglecting the differential and (if present) the higher-harmonic cyclic components, for $N_0^r = N_c^r = N_s^r = 1$, $\phi_1^0 = 1$, and $\phi_1^c = \phi_1^s = r$, the proposed inflow distribution coincides with the Pitt-Peters model [1, 2], while the combination of Eq. 1 with the expressions of the inflow coefficients in Eq. 2 is closely related to the approximation form applied in the Peters-He model [3].

Once the inflow distribution history is known from aerodynamics simulation, at

each time step, $\bar{t}$, the inflow coordinates of the α inflow coefficient are given by the following least-square evaluation approach

$$\begin{bmatrix} \lambda_1^\alpha(\bar{t}) \\ \lambda_2^\alpha(\bar{t}) \\ \vdots \\ \lambda_{N_\alpha^r}^\alpha(\bar{t}) \end{bmatrix} = [\boldsymbol{\Phi}^\alpha]^{-1} \boldsymbol{\nu}^\alpha(\bar{t}) \tag{3}$$

where $\boldsymbol{\Phi}^\alpha$ is the matrix of the inner product of the radial shape functions, namely such that $\Phi_{ij}^\alpha = <\phi_i^\alpha(r), \phi_j^\alpha(r)>$, whereas $\boldsymbol{\nu}^\alpha$ is the vector collecting the projections of the inflow coefficient onto the radial shape functions, namely $\nu_i^\alpha(\bar{t}) = <\nu_\alpha(r,\bar{t}), \phi_i^\alpha(r)>$.

When rotors are in steady flight conditions, the inflow on each blade (rotating frame observer) is periodic with non-zero mean value and fundamental frequency equal to the rotational frequency, Ω. The corresponding collective and cyclic coefficients in Eq. 2 (non-rotating frame observer) are periodic with non-zero mean value and fundamental frequency equal to $N_b\,\Omega$, whereas the differential coefficient (if present) has null mean value and harmonic components at the frequencies $(1/2+m)N_b\Omega$, for $m = 0, 1, ..., M$, with M related to the maximum order of periodicity of the aerodynamic operator. Exceptions are the axi-symmetric cases, for which the inflow is constant in both frames.

Because of this periodic nature of rotor aerodynamics, even a small single-harmonic disturbance of the operating conditions (*i.e.,* such to produce negligible nonlinear effects) yields multi-harmonic inflow perturbations. For instance, for a small-perturbation harmonic collective/cyclic input of frequency ω, non-zero harmonic components of the corresponding perturbations of collective/cyclic inflow coefficients appear at the frequencies ω and $mN_b\Omega \pm \omega$, for $m = 1, 2, ..., M$, whereas non-zero harmonic components of the differential inflow coefficient perturbation appear at the frequencies $(1/2 + m)N_b\Omega \pm \omega$, for $m = 0, 1, ..., M$. In the rotating frame, the inflow presents harmonic components at ω and $k\Omega \pm \omega$, for $k = 1, 2, ..., MN_b$.

This is confirmed by the results presented in Figures 1 and 2 obtained through the BEM free-wake solver for potential flows presented in [21], that concern the inflow evaluated on the four-bladed Bo-105 main rotor operating in momentum trim condition, with thrust $T = 22000$ N, advance ratio $\mu = 0.2$ and angular speed $\Omega = 44.4$ rad/s.

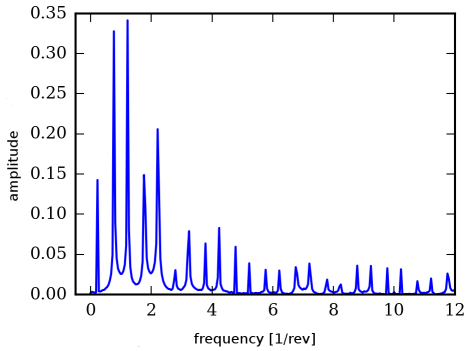

Figure 1: Blade inflow perturbation spectrum at $r/R = 0.7$, for small-amplitude, harmonic θ_s. $\mu = 0.2$.

Specifically, Figure 1 shows the spectrum of the perturbed inflow on a generic blade at radial position $r/R = 0.7$ due to a small-amplitude harmonic longitudinal pitch, θ_s, oscillating with frequency $\omega = 0.225\,\Omega = 10$ rad/s. whereas Figure 2 presents the spectra of the corresponding perturbed inflow coefficients.

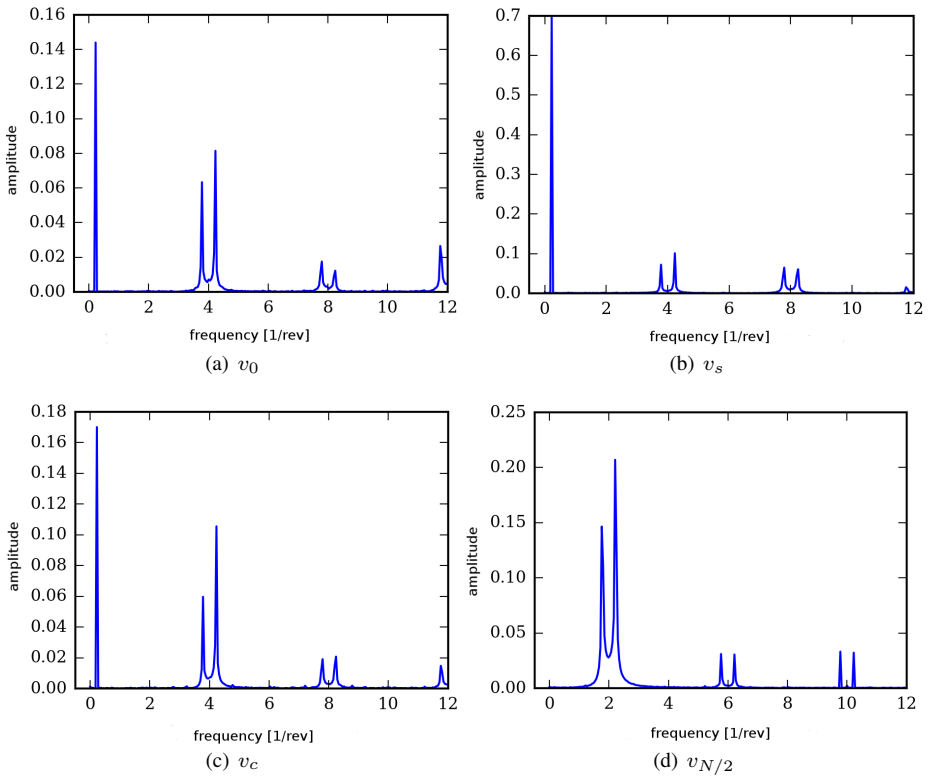

(a) v_0 (b) v_s

(c) v_c (d) $v_{N/2}$

Figure 2: Spectra of inflow coefficients at $r/R = 0.7$, for small-amplitude, harmonic θ_s. $\mu = 0.2$.

Indeed, from Figure 1 it is possible to notice that, in the rotating frame, the perturbed inflow spectrum is characterized by a peak at 0.225/rev and couples of peaks around multiples of the rotor revolution frequency, whereas peaks due to nonlinearities (that would appear at multiples of the perturbation frequency) are not visible because of the small amplitude of perturbations. Since the input is a cyclic command, the highest peaks are those around Ω (namely, those at 0.775/rev and 1.225/rev in Figure 1), and this proves the unsuitability of representing rotor inflow in the rotating frame through a simple (not multi-harmonic, see later) LTI model, in that it would be capable of taking into account only the ω component of the output.

Instead, Figure 2 shows that the spectra of collective and cyclic inflow coefficients are characterized by a significant tonal peak at the input frequency (particularly for ν_s), with progressively smaller peaks around the multiples of $N_b\,\Omega$. This explains the satisfactory accuracy of the dynamic inflow models based on simple LTI description of the non-rotating-frame inflow coefficients like, for instance, the Pitt-Peters one. However, at the same time, the higher frequency components of the cross-coupling terms (namely, those different from ν_s, with inclusion of $\nu_{N/2}$) are not negligible with respect to the input frequency ones. These are not captured by simple LTI inflow coefficient models, and this limits their accuracy for applications where high-frequency dynamics is present (like, for instance, in rotor blade aeroelasticity and aggressive maneuver dynamic responses).

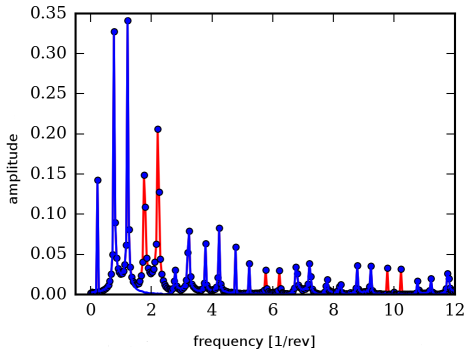

Figure 3: Correlation among spectra of rotating-frame inflow perturbation at $r/R = 0.7$: computed inflow (●), inflow representation in Eq. 1 with (——) and without (——) differential contribution.

The importance of the introduction of the differential inflow coefficient in the inflow representation is demonstrated in Figure 3, where the spectrum of the computed rotor blade inflow (blue circles) is compared with those of the inflows given by the expression in Eq. 1 with (red line) and without (blue line) inclusion of the $\nu_{N/2}$ term. Indeed, it shows that not-negligible output harmonic content around frequency $(N_b/2)\Omega$ is missing if the differential contribution is not taken into account.

Finally, note that in case of harmonic perturbation inputs of differential type, the collective/cyclic coefficients of the corresponding inflow perturbation have harmonic peaks at the same frequencies of the peaks in Figure 2(d), whereas the differential coefficient presents a spectrum distribution similar to those in Figures 2(a) to 2(c).

2.2. Multi-Harmonic Representation of Inflow Coordinates

Based on the above observations, for the purpose of deriving LTP inflow models by combination of LTI dynamics, it is convenient to express each inflow coordinate, λ_j^α, through one of the following time-dependent multi-harmonic combinations

$$\begin{cases} \lambda_j^\alpha(t) = \lambda_j^{\alpha,0}(t) + \displaystyle\sum_{m=1}^{M} \left\{ \lambda_j^{\alpha,mc}(t) \cos(m\,\Omega_b\,t) + \lambda_j^{\alpha,ms}(t) \sin(m\,\Omega_b\,t) \right\} & (4) \\ \lambda_j^\alpha(t) = \displaystyle\sum_{m=0}^{M} \left\{ \lambda_j^{\alpha,mc}(t) \cos\left((1/2+m)\,\Omega_b\,t\right) + \lambda_j^{\alpha,ms}(t) \sin\left((1/2+m)\Omega_b\,t\right) \right\} & (5) \end{cases}$$

where $\Omega_b = N_b\,\Omega$. The expression in Eq. 4 is suitable to represent both collective/cyclic responses to fixed-frame/collective/cyclic inputs and differential responses to differential inputs, whereas the expression in Eq. 5 is valid both for collective/cyclic responses to differential inputs and for differential responses to fixed-frame/collective/cyclic inputs.

Note that, considering a small-perturbation harmonic collective/cyclic input at a given frequency, ω, the generic inflow coordinate, λ_j^α, of a collective/cyclic output perturbation is such that its ω-harmonic components coincide with those of $\lambda_j^{\alpha,0}$ (see Eq. 4 and Figures 2(a) to 2(c)), whereas from the combination of its $(m\,\Omega_b - \omega)$- and $(m\,\Omega_b + \omega)$-harmonic components it is possible to determine the ω-harmonic components of $\lambda_j^{\alpha,mc}$ and $\lambda_j^{\alpha,ms}$ (similar considerations are valid for the input/output relations represented by Eq. 5).

This implies that, from numerical simulations of a high-fidelity aerodynamic solver, it is possible to extract the LTI operators relating small input perturbations to the multi-harmonic coefficients of the inflow coordinates in Eq. 4 or 5. Indeed, the combination of the ω-harmonic components of $\lambda_j^{\alpha,0}$, $\lambda_j^{\alpha,mc}$, $\lambda_j^{\alpha,ms}$ with the harmonic components of the input readily provides the values of the input/multi-harmonic-coefficients transfer functions $H_{jk}^{\alpha,0}(\omega)$, $H_{jk}^{\alpha,mc}(\omega)$, $H_{jk}^{\alpha,ms}(\omega)$ and this process can be repeated for a suitable set of points within the frequency range of interest.

2.3. Efficient Extraction of Multi-Harmonic Coefficients LTI Dynamics

However, the application of a set of mono-harmonic perturbations for each input variable is not the most suitable way to identify all transfer functions involved in the proposed multi-harmonic description of the dynamic inflow (for instance, the coalescence of contributions occurring for $\omega = \Omega/2$ would bring to undetermined values of the transfer functions).

Here, an efficient methodology for the extraction of the transfer functions is proposed. It is based on the fundamental property of LTP operators according to which their output spectrum depends not only on the frequency of the input signal, but also on its time shift (delay) with respect to the system intrinsic period [22]. Specifically, given, for instance, a rotor kinematic collective/cyclic input, the corresponding inflow collective/cyclic output representation in Eq. 4 is suitably extended as follows

$$\begin{aligned} \lambda_j^{\alpha}(t,\tau) \;&=\; \lambda_j^{\alpha,0}(t) \\ &+\; \sum_{m=1}^{M} \left\{ \lambda_j^{\alpha,mc}(t)\cos(m\,\Omega_b\,(t+\tau)) \,+\, \lambda_j^{\alpha,ms}(t)\sin(m\,\Omega_b\,(t+\tau)) \right\} \end{aligned} \tag{6}$$

where τ denotes the input/system-period time shift, which characterizes the corresponding output (this extension is similarly applicable also to the representation in Eq. 5).

Then, note that, the evaluation of $\lambda_j^{\alpha}(t,\tau)$ for a discrete set of N_τ values $\tau = \tau_i$, for any time $t = \bar{t}$ yields a set of N_τ linearly independent equations with unknowns $\lambda_j^{\alpha,0}(\bar{t}), \lambda_j^{\alpha,mc}(\bar{t}), \lambda_j^{\alpha,ms}(\bar{t})$. Hence, the transfer functions $H_{jk}^{\alpha,0}, H_{jk}^{\alpha,mc}, H_{jk}^{\alpha,ms}$ introduced in Section 2.2 are efficiently identified through the following process:

- for each input variable, the rotor is perturbed by a sequence of $N_\tau \geq (2M+1)$

chirp signals differing for the time delays, $\tau_i = iT/N_\tau$, with $i = 1, ..., N_\tau$ and T denoting the fundamental intrinsic period of the system, $T = 2\pi/\Omega_b$;

- considering a suitable time interval of analysis (depending on the spectrum to be identified), for a given discrete set of time instants, $\bar{t}$, within it, it is possible to determine the corresponding values of each multi-harmonic coefficient as solutions of the following algebraic problem

$$\mathbf{P}(\bar{t}) \begin{bmatrix} \lambda_j^{\alpha,0}(\bar{t}) \\ \lambda_j^{\alpha,1c}(\bar{t}) \\ \lambda_j^{\alpha,1s}(\bar{t}) \\ \vdots \\ \lambda_j^{\alpha,Mc}(\bar{t}) \\ \lambda_j^{\alpha,Ms}(\bar{t}) \end{bmatrix} = \begin{bmatrix} \lambda_j^{\alpha}(\bar{t},\tau_1) \\ \lambda_j^{\alpha}(\bar{t},\tau_2) \\ \lambda_j^{\alpha}(\bar{t},\tau_3) \\ \vdots \\ \lambda_j^{\alpha}(\bar{t},\tau_{N_\tau}) \end{bmatrix} \tag{7}$$

where $\mathbf{P}$ is a matrix of size $[N_\tau \times (2M+1)]$, with entries defined as

$$\begin{cases} P_{i1} = 1 \\ P_{in}(\bar{t}) = \cos\left(\dfrac{n}{2}\Omega_b(\bar{t}+\tau_i)\right), & \text{for } n \text{ even} \\ P_{in}(\bar{t}) = \sin\left(\dfrac{n-1}{2}\Omega_b(\bar{t}+\tau_i)\right), & \text{for } n \text{ odd} \end{cases}$$

(for $N_\tau > (2M+1)$ the problem in Eq. 7 is solved through pseudo-inversion of matrix $\mathbf{P}$);

- once the necessary evaluations in the considered time interval are accomplished, the transfer function between each multi-harmonic coefficient and the specific input considered is determined (frequency by frequency) as the ratio between the respective discrete Fourier transforms.

Note that, a similar procedure is applicable for the identification of the i/o transfer functions related to the multi-harmonic representation in Eq. 5.

For the purpose of experimental identification of a helicopter rotor system, an approach related to the present one is applied in [23, 24], with the multi-harmonic coefficients problem formulated in the frequency domain instead of time-domain, as in Eq. 7.

2.4. Finite-State Approximation

In order to derive a finite-state modeling of the wake inflow, the LTI dynamics of the multi-harmonic coefficients in Eqs. 4 and 5 (collected in the vector $\boldsymbol{\lambda}_j^\alpha$) is conveniently represented through the following assembled transfer-matrix form

$$\tilde{\boldsymbol{\lambda}}_j^\alpha = \mathbf{H}_j^\alpha(s)\,\tilde{\mathbf{q}} \tag{8}$$

where s is the Laplace-domain variable, $\mathbf{q}$ denotes the vector of the inputs of interest, whereas the matrix $\mathbf{H}_j^\alpha$ collects the corresponding transfer functions extracted from the aerodynamic responses through the procedure outlined above.

Then, observing that the input vector may be composed of velocity and/or displacement variables, and that the output vector is composed of induced velocity coefficients, this matrix is approximated through the following rational-matrix form

$$\mathbf{H}_j^\alpha\,(s) \approx s\;\mathbf{A}_1 + \mathbf{A}_0 + \mathbf{C}\left[s\;\mathbf{I} - \mathbf{A}\right]^{-1}\;\mathbf{B} \tag{9}$$

determined by a least-square technique as that providing the best fitting of the values of the matrix $\mathbf{H}_j^\alpha$ (samples) derived from solutions of Eq. 7 [19, 25]. Matrices $\mathbf{A}_1, \mathbf{A}_0, \mathbf{B}$ and $\mathbf{C}$ are real and fully populated, whereas $\mathbf{A}$ is a square block-diagonal matrix containing the poles of the approximated transfer functions.

Finally, transforming into time domain the combination of Eqs. 8 and 9 provides the following LTI, finite-state model of the wake inflow multi-harmonic coefficients

$$\boldsymbol{\lambda}_j^\alpha = \mathbf{A}_1\,\dot{\mathbf{q}} + \mathbf{A}_0\,\mathbf{q} + \mathbf{C}\,\mathbf{r} \tag{10}$$

$$\dot{\mathbf{r}} = \mathbf{A}\,\mathbf{r} + \mathbf{B}\,\mathbf{q} \tag{11}$$

where $\mathbf{r}$ is the vector of the additional wake inflow dynamics states.

The above LTI differential model combined with Eqs. (4) and (5) provides the LTP operator for the wake inflow coordinates. These, in turn, applied for all j and α in Eq. 2 coupled with Eq. 1 yield a space-time accurate, LTP prediction model of the wake inflow on the rotor disc, suitable for rotorcraft aeroelastic and flight dynamics applications.

If the multi-harmonic terms in Eqs. 4 and (5) are neglected, the operator relating wake inflow coordinates to rotor kinematics perturbations is transformed into an oper-

ator of LTI type, like that of the wake inflow model extraction approach introduced in [13, 15] for low-frequency flight dynamics applications.

2.5. Application to coaxial rotors

The wake inflow modeling outlined above may be straightforwardly extended to coaxial rotors. In this case, the input kinematic variables might include blade pitch controls for both rotors, whereas the inflow coefficients are doubled in order to represent the inflow distributions over upper and lower rotor discs.

For an isolated system of contra-rotating coaxial rotors, in the non-rotating frame the fundamental frequency of both upper and lower wake inflows is $2\Omega_b$ in hovering conditions, and Ω_b when it is in forward flight. The methodology presented above can be correspondingly adapted for their finite-state, space-time accurate modeling.

Note that, the introduction of fuselage interaction effects would cause the loss of axial-symmetry existing in isolated hovering condition, thus moving the fundamental frequency from $2\Omega_b$ to Ω_b.

3. Numerical results

The proposed methodology for space-time accurate, finite-state, dynamic wake inflow modeling is verified and validated for a single rotor in hovering condition (time-constant aerodynamic operator, multi-harmonic coefficients not included) and a coaxial rotor configuration in hovering and forward flight (multi-harmonic coefficients duly included in both cases).

The aerodynamic simulations used for inflow models extraction are obtained by an unsteady, free-wake, potential-flow, BEM tool for rotorcraft extensively validated in the past by some of the authors [21, 26], that is capable of taking into account multi-body interference and severe blade-vortex interaction effects.

Dividing the blade span into a finite number of segments, the basis functions used in Eq. 2 are assumed to be equal for the different inflow coefficients (namely, $\phi_j^0 = \phi_j^c = \phi_j^s = \phi_j^{N/2}, \forall j$) and such to provide a linear distribution of inflow coefficients within each segment, assuring continuity at the edges of them. For the results presented in the following, four discretization segments are used ($N_0^r = N_c^r = N_s^r = N_{N/2}^r = 4$).

3.1. Single rotor in hovering condition

The rotor examined has four blades, radius $R = 4.91$ m, constant chord $c = 0.27$ m, twist angle $\theta_{tw} = -8^\circ$ from root to tip, and angular speed $\Omega = 44.4$ rad/s.

For the sake of simplicity (and with no loss of generality in terms of inflow modeling technique validation), the rotor wake in the aerodynamic BEM solver is assumed to have a prescribed helicoidal shape, with spiral length given by the mean inflow associated to the thrust coefficient, C_T, such that $C_T/\sigma = 0.07$, with σ denoting the rotor solidity.

First, the excellent quality of the rational-matrix approximation (RMA) of the transfer function matrix extracted from the BEM solutions is shown in Figures 4(a) and 4(b), which present the spectra of λ_1^0 *vs* θ_0 and λ_1^s *vs* θ_c, respectively (note that, in this case, $\lambda_1^0 \equiv \lambda_1^{0,0}$ and $\lambda_1^s \equiv \lambda_1^{s,0}$, see Eq. 4).

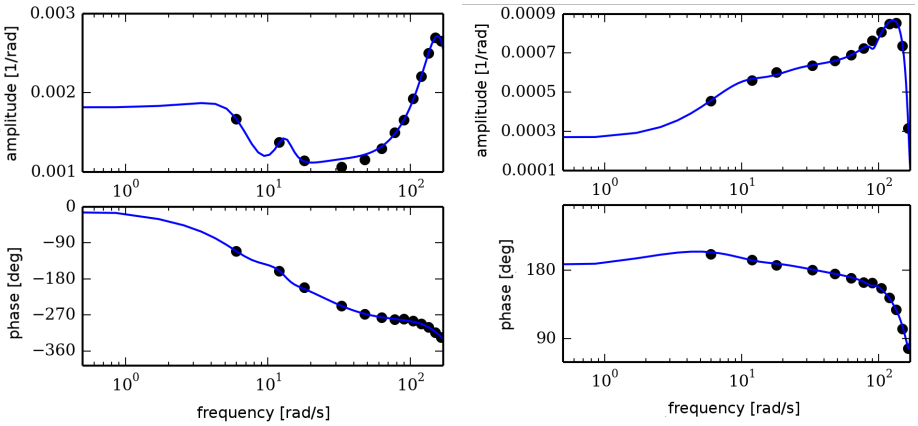

(a) λ_1^0 *vs* θ_0 (b) λ_1^s *vs* θ_c

Figure 4: Single rotor in hover, transfer function of inflow coordinates. — RMA; ● BEM.

A similar high level of accuracy is observed for the whole set of transfer functions involved in matrices $\mathbf{H}_j^\alpha$.

Next, considering a collective pitch chirp-type perturbation with 1-deg amplitude and frequency linearly increasing in the range $[0 \div 0.3]$/rev, the corresponding wake inflow perturbation predicted by the proposed state-space model is correlated both with those directly computed by the BEM solver and with those given by the inflow model of [13, 14], based on the linear radial approximation form (like in the Pitt-Peters model).

This comparison is shown in Figure 5 for the wake inflow evaluated at three blade sections, $r/R = \{0.7, 0.85, 0.95\}$.

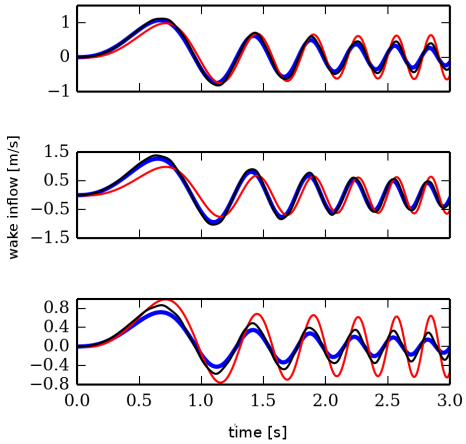

Figure 5: Single rotor in hover, wake inflow at $r/R = 0.7$ (top), $r/R = 0.85$, $r/R = 0.95$ (bottom), due to collective pitch perturbation. BEM; present model; linear radial approximation.

These results demonstrate the improvement of the quality of the dynamic model predictions obtained by introduction in Eq. 2 of a more accurate representation of the inflow radial distribution that, especially at the tip of the blade, shows significant gradients.

This is confirmed by the results shown in Figure 6 that presents the spanwise distribution of the percentage root-mean-square (RMS) prediction error (related to the sectional inflow peak) obtained by the present formulation and by the model with linear radial approximation of [14]. The inflow prediction improvement provided by the more accurate radial description is considerable throughout the blade span.

3.2. Coaxial rotors inflow approximation

The coaxial rotor system examined is composed of two identical three-bladed rotors having radius $R = 5.48$ m, blade root chord $c = 0.54$ m, taper ratio equal to 0.5, twist $\theta = -7°$, counter-rotating at angular velocity $\Omega = 32.8$ rad/s.

Akin to the single rotor analysis, the rotor wake in the aerodynamic BEM solver is assumed to have a prescribed helicoidal shape that, for the hovering case has a spiral

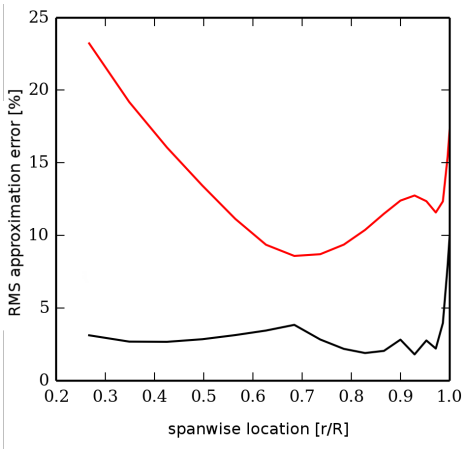

Figure 6: Single rotor in hover, RMS inflow approximation error. present model; linear radial approximation.

length related to the mean thrust coefficient, whereas in forward flight (without loss of generality, $\mu = 0.2$ is the case examined here) coincides with the surface swept by the trailing edges. In both cases, the reference operating condition is characterized by $C_T = 0.0134$ and null rolling and pitching moments (momentum trim condition).

First of all, the capability of the applied inflow representation to approximate with suitable accuracy the inflow predicted by the BEM solver is verified. Figure 7 depicts the inflow on upper and lower rotor blades in forward flight evaluated by the aerodynamic solver, as responses to a steady differential collective perturbation (namely a collective pitch perturbation of opposite sign on upper and lower rotors). It shows irregular distributions characterized by the strong influence of tip vortices (proven by the curvilinear traces of higher velocity gradient) that could not be accurately approximated by linear models like that in [14] or the Pitt-Peters one.

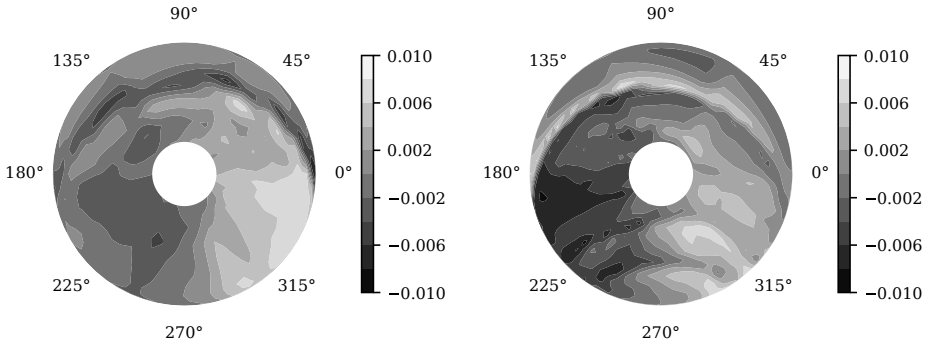

(a) upper rotor (b) lower rotor

Figure 7: BEM prediction of wake inflow distribution due to differential collective perturbation.

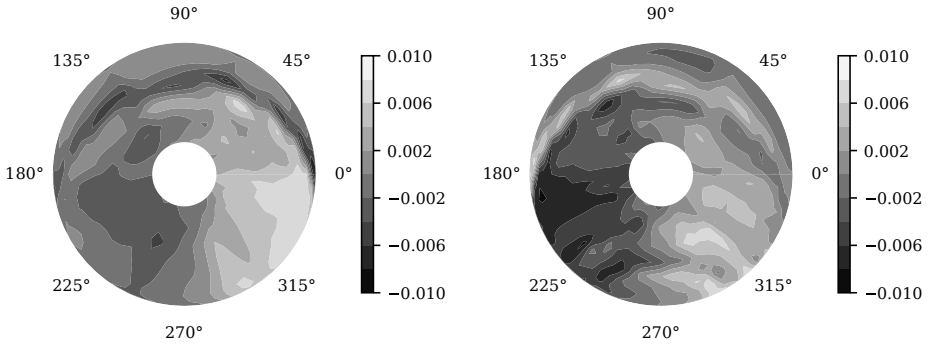

(a) upper rotor (b) lower rotor

Figure 8: Analytical representation of wake inflow distribution due to differential collective perturbation.

Instead, the model proposed here, for $M = 2$ and the number of radial functions mentioned above, provides the inflow approximation presented in Figure 8. Of course, it could be further enhanced by increasing the number of radial functions and multi-harmonic coefficients, but it is considered of satisfactory quality and represents a good trade-off between accuracy and complexity of the analytical model. Indeed, a more complex inflow representation would imply higher computational cost for the identification of the finite-state models and a higher number of additional inflow states to be introduced. For these reasons, the results presented in the following are based on these model discretization parameters when concerning advancing rotor system, whereas $M = 1$ is used for hovering condition.

3.3. Coaxial rotors in hovering condition

First, the good quality of the RMA of the transfer functions extracted from the BEM solver is demonstrated in Figure 9, which presents the spectrum of $\lambda_2^{0,0}$ *vs* θ_0^+ (with θ_0^+ denoting the average of upper and lower rotor collective pitches). A similar level of accuracy is observed for all of the multi-harmonic coefficient transfer functions.

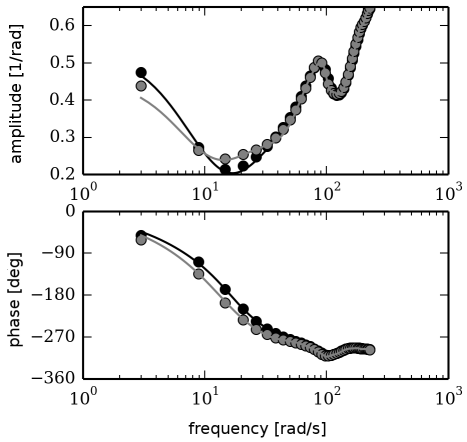

Figure 9: Coaxial rotor system in hover, transfer function $\lambda_2^{0,0}$ *vs* θ_0^+. Upper rotor: ——— RMA; ● BEM. Lower rotor: ——— RMA; ● BEM.

Next, considering the following time history of θ_0^+ perturbations

$$\theta_0^+(t) = A\cos(\omega t)\sin(3\omega t)e^{-0.25t} \tag{12}$$

with $A = 0.5$ deg and $\omega = 0.1\Omega$, the corresponding wake inflow perturbations predicted by the proposed state-space methodology are correlated both with those directly computed by the BEM solver and with those predicted by a linear-radial-approximation dynamic inflow model obtained following the formulation in [13, 14]. This comparison is presented in Figure 10 in terms of the wake inflow evaluated at the blade sections $r/R = \{0.41, 0.62, 0.95\}$, on upper and lower rotor blades.

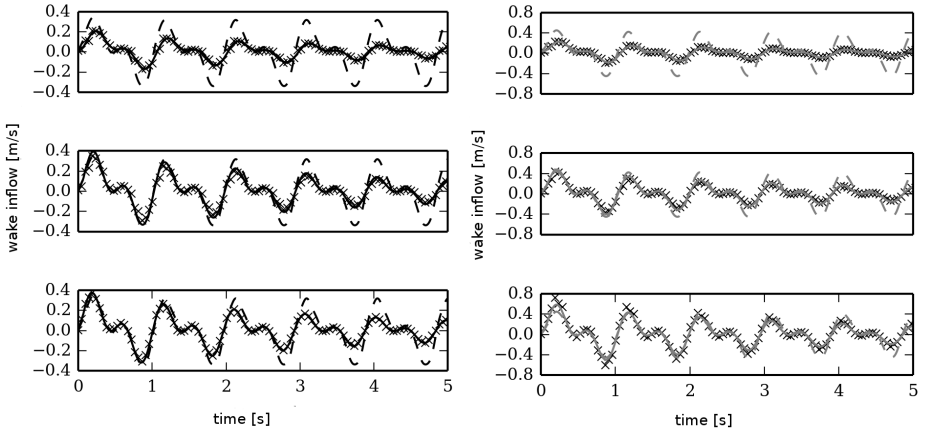

(a) upper rotor (b) lower rotor

Figure 10: Coaxial rotor system in hover, wake inflow predictions at $r/R = 0.41$ (top), $r/R = 0.62$, $r/R = 0.95$ (bottom). $\times\times$ BEM; ——— present model; - - - linear radial approximation.

330 This figure shows that the present model provides inflow predictions that almost perfectly match those directly given by the aerodynamic solver, thus significantly improving those from the linear radial approximation model.

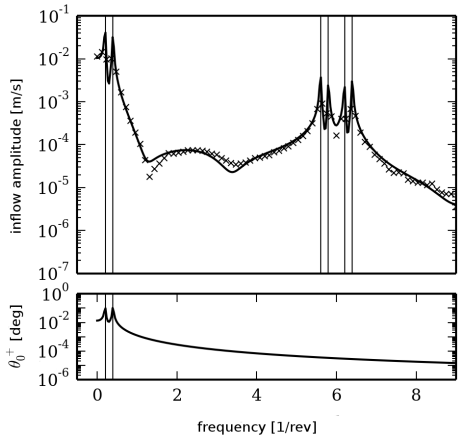

Figure 11: Coaxial rotor system in hover, wake inflow spectrum at $r/R = 0.41$, upper rotor. $\times\times$ BEM; ——— present model.

The very good quality of present model predictions is confirmed in Figure 11, which shows the correlation with BEM simulations in terms of the spectrum of the upper

rotor inflow at $r/R = 0.41$. In particular, it is interesting to note that, although of smaller amplitudes, also the contributions deriving from the 6/rev periodicity of the aerodynamic operator are very well captured by the proposed methodology.

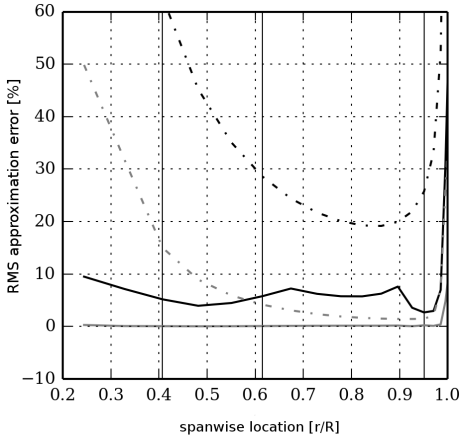

Figure 12: Coaxial rotor system in hover, RMS inflow approximation error. Upper rotor: present model; linear radial approximation. Lower rotor: present model; linear radial approximation.

An overview of the quality of the model proposed is given in Figure 12. It presents the spanwise distributions of the percentage RMS error with respect to BEM predictions (related to the sectional inflow peak), obtained by the present formulation and by that based on the linear radial approximation. Indeed, the error of the present model predictions is below 10% throughout the blade span for both upper and lower rotors (except at the outermost region), and is less than half of that given by the linear radial model. Note that the vertical solid lines identify the blade sections examined in Figure 10, and that the higher error at the blade tip region is caused by the local very high inflow gradients that, however, could be better captured by suited local refinement of the radial approximation functions.

3.4. Coaxial rotors in forward flight

As already observed, in forward flight condition the fundamental frequency of the intrinsic periodicity of the aerodynamic operator is 3Ω, the harmonic content is en-

riched by higher-frequency contributions, and thus, the inflow model includes the multi-harmonic coefficients corresponding to $M = 2$ in Eqs. 4 and 5.

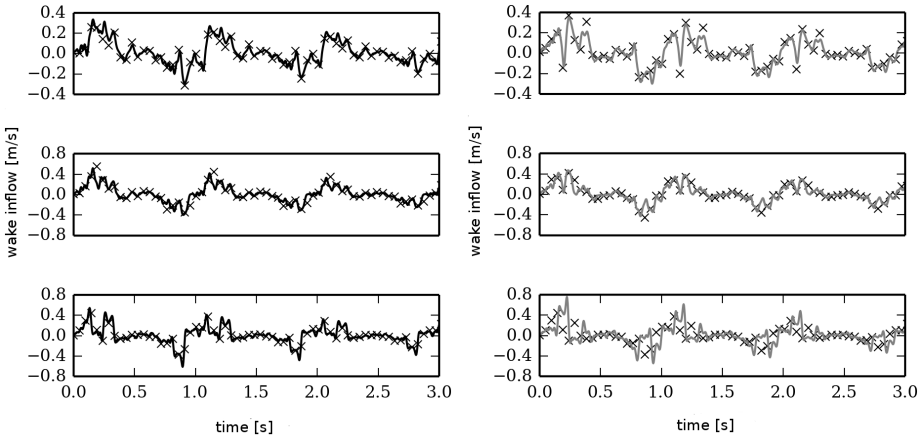

(a) upper rotor (b) lower rotor

Figure 13: Coaxial rotor system in forward flight, wake inflow predictions at $r/R = 0.41$ (top), $r/R = 0.62$, $r/R = 0.95$ (bottom). $\times\times$ BEM; ——— present model.

Considering again the perturbation input of Eq. 12, for upper and lower rotors, Figure 13 shows the comparisons between the wake inflow predicted by the present dynamic model and that directly provided by the BEM solver on the same three blade sections examined for the hovering case. The two simulations are in good agreement (particularly those concerning the upper rotor, which are practically coinciding), thus proving the capability of the space-time-accurate, finite-state model to describe with good level of accuracy the wake inflow field over rotor systems.

It is interesting to note that, contrarily to the outcomes observed for the hovering system, in forward flight condition the time periodicity of the aerodynamic operator heavily affects the output. This is particularly evident in Figure 14 which presents the frequency spectrum of the upper rotor inflow coordinate λ_3^s proving, also in this case, the good correlation between BEM output and model predictions. Indeed, in this case, the amplitude of the multi-harmonic components associated to the 3/rev periodicity of the aerodynamic operator are of the same order of magnitude of the LTI components (namely, those at the same frequencies of the input). Even the multi-harmonic components derived from the 6/rev intrinsic periodicity provide a not negligible contribution

(also lower contributions from the 9/rev periodicity can be observed in the BEM output, not captured by the analytical model in that developed for $M = 2$).

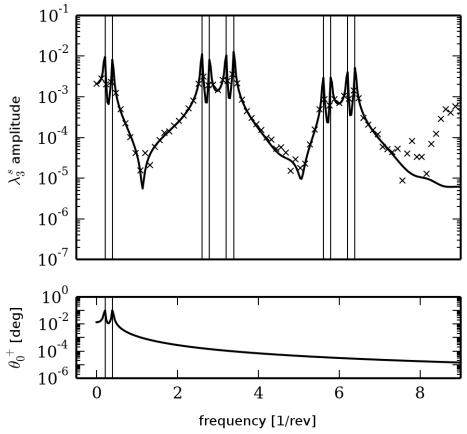

Figure 14: Coaxial rotor system in forward flight, spectrum of upper rotor inflow coordinate λ_3^s. $\times\times$ BEM; —— present model.

Finally, for upper and lower rotors Figure 15 shows the spanwise distribution of the percentage RMS error with respect to BEM predictions (related to the sectional inflow peak) corresponding to inflow given by (i) complete present model, (ii) present model without multi-harmonic terms (LTI representation of inflow coordinates), (iii) linear radial approximation model of [13, 14]. In addition, it depicts also the modeling error arising when the inflow coordinates are evaluated directly from BEM simulations, and hence related only to the proposed approximation of the radial inflow distribution.

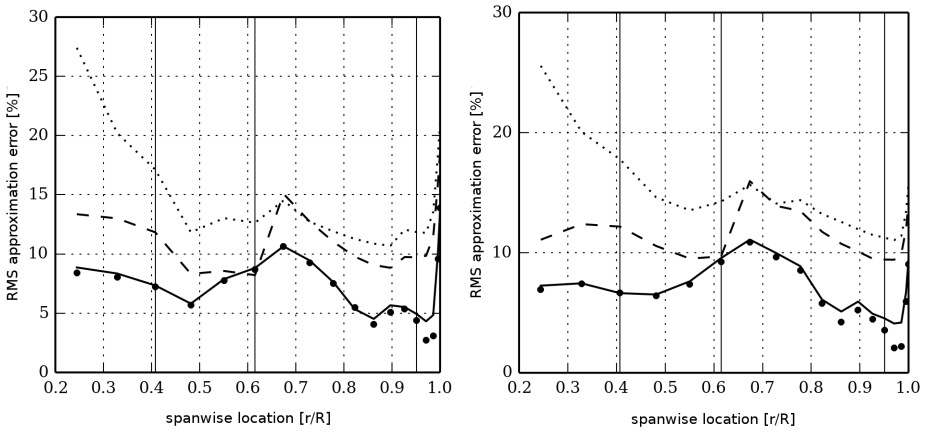

(a) upper rotor (b) lower rotor

Figure 15: Coaxial rotor system in forward flight, RMS inflow approximation error. ——— present model (complete); – – – present model (w/o multi-harmonic terms); ····· linear radial approximation; ● inflow coordinates from BEM.

This figure proves that, introducing only a more detailed radial description without including multi-harmonics contributions yields limited improvements of the overall quality of the inflow predictions, as compared to those of the linear radial approximation model of [13, 14]. This confirms that for forward flight conditions, combined space-time accurate descriptions are required for high-quality inflow modeling. Moreover, the comparison of the complete model predictions with those obtained through inflow coordinates directly evaluated from BEM outputs demonstrates that the proposed finite-state modeling process (harmonics truncation, transfer functions identification, rational matrix approximation) does not introduce significant errors which, instead, are closely related to the quality of the inflow radial distribution description.

4. Conclusions

A methodology for the extraction of space-time accurate, finite-state, LTP rotor inflow dynamic models from high-fidelity aerodynamic solvers has been introduced. Its numerical assessment has been performed through applications to single and coaxial rotors, both in hovering and forward flight. The following conclusion are drawn:

- the proposed methodology is capable of simulating high-frequency, multi-harmonic rotor inflow through a LTP operator forced by rotor kinematics;
- it suitably captures the effects of the intrinsic periodicity of rotor aerodynamics (always present, unless a single isolated rotor in hovering/axial flow is considered);
- it is applicable to inflow observed both in the rotating frame and in the non-rotating one; however, the inflow description in the non-rotating frame turns out more convenient in that, given the highest frequency to be taken into account, it requires the introduction of a lower number of multi harmonics;
- the proposed inflow modeling technique can be successfully applied both to single rotors and coaxial-rotor configurations, both in hovering and forward flight conditions;
- the accuracy of the model can be adjusted by suitable radial discretization (number of inflow coordinates) and multi-harmonic expansion (number of multi-harmonic coefficients);
- significant improvements with respect to LTI, linear radial approximation models (like the widely-applied Pitt-Peters model) are achieved both because of the description of the radial distribution as a linear combination of suitable basis functions, and because of the multi-harmonic expansion of the corresponding inflow coordinates;
- transfer function identification and rational approximation can be accomplished with a very good level of accuracy.

The capability of capturing with good accuracy both radial inflow distribution and inflow higher-order harmonic content makes the proposed dynamic inflow modeling methodology suitable for effectively introducing the unsteady aerodynamics effects in rotorcraft aeromechanics simulations.

References

[1] D. M. Pitt, D. A. Peters, Theoretical Predictions of Dynamic Inflow Derivatives, Vertica 5 (1981) 21–34.

[2] D. A. Peters, N. HaQuang, Dynamic inflow for practical applications, Journal of American Helicopter Society 33 (4) (1988) 64–68.

[3] D. A. Peters, C. J. He, Correlation of measured induced velocities with a finite-state wake model, Journal of the American Helicopter Society 36 (3) (1991) 59–70.

[4] A. Rosen, A. Isser, A new model of rotor dynamics during pitch and roll of a hovering helicopter, Journal of the American Helicopter Society 40 (3) (1995) 17–28.

[5] K. R. Krothapalli, P. J. V. R, D. A. Peters, Study of a rotor flap-inflow model including wake distortion terms, in: RTO SCI Symposium on "System Identification for Integrated Aircraft Development and Flight Testing", Madrid, Spain, 1998.

[6] U. T. Arnold, J. D. Keller, H. Curtiss, G. Reichert, et al., The effect of inflow models on the predicted response of helicopters, Journal of the American Helicopter Society 43 (1) (1998) 25–36.

[7] R. E. Brown, Rotor wake modeling for flight dynamic simulation of helicopters, AIAA journal 38 (1) (2000) 57–63.

[8] J. Prasad, M. Nowak, H. Xin, Finite state inflow models for a coaxial rotor in hover, in: Proceedings of 38th European Rotorcraft Forum, Amsterdam, The Netherlands, 2012.

[9] M. Nowak, J. Prasad, D. Peters, Development of a finite state model for a coaxial rotor in forward flight, in: American Helicopter Society 70th Annual Forum, Quebec, Canada, 2014.

[10] Y. Kong, J. Prasad, L. Sankar, J. Kim, Finite state coaxial rotor inflow model improvements via system identification, in: American Helicopter Society 72th Annual Forum, West Palm Beach, FL, 2016.

[11] A. Su, K. M. Yoo, D. A. Peters, Extension and validation of an unsteady wake model for rotors, Journal of aircraft 29 (3) (1992) 374–383.

[12] D. A. Peters, How dynamic inflow survives in the competitive world of rotorcraft aerodynamics, Journal of the American Helicopter Society 54 (1) (2009) 11001.

[13] M. Gennaretti, R. Gori, J. Serafini, G. Bernardini, F. Cardito, Rotor dynamic wake inflow finite-state modelling, in: 33rd AIAA Applied Aerodynamics Conference, Dallas, TX, 2015.

[14] M. Gennaretti, R. Gori, J. Serafini, F. Cardito, G. Bernardini, Identification of rotor wake inflow finite-state models for flight dynamics simulations, CEAS Aeronautical Journal 8 (1) (2017) 209–230.

[15] F. Cardito, R. Gori, G. Bernardini, J. Serafini, M. Gennaretti, Finite-state dynamic wake inflow modelling for coaxial rotors, in: 41^{st} European Rotorcraft Forum, Munich, Germany, 2015.

[16] F. Cardito, R. Gori, J. Serafini, G. Bernardini, M. Gennaretti, State-space coaxial rotors inflow modelling derived from high-fidelity aerodynamic simulations, CEAS Aeronautical Journal 9 (4) (2018) 587–606.

[17] O. Rand, V. Khromov, S. Hersey, R. Celi, O. Juhasz, M. Tischler, Linear inflow model extraction from high-fidelity aerodynamic models for flight dynamics applications, in: 71st Annual Forum of the American Helicopter Society, Virginia Beach, VA, 2015.

[18] O. Rand, V. Khromov, Free-wake–based dynamic inflow model for hover, forward, and maneuvering flight, Journal of the American Helicopter Society 63 (1) (2018) 1–16.

[19] M. Gennaretti, D. Muro, Multiblade reduced-order aerodynamics for state-space aeroelastic modeling of rotors, Journal of Aircraft 49 (2) (2012) 495–502.

[20] R. Gori, J. Serafini, M. Molica Colella, M. Gennaretti, Assessment of a State—Space Aeroelastic Rotor Model for Rotorcraft Dynamics Analysis, in: Proceedings of the XXII AIDAA Conference, Naples, Italy, 2013.

[21] M. Gennaretti, G. Bernardini, Novel boundary integral formulation for blade-vortex interaction aerodynamics of helicopter rotors, AIAA Journal 45 (6) (2007) 1169–1176.

[22] N. M. Wereley, S. R. Hall, Frequency response of linear time periodic systems, in: Proceedings of the 29th IEEE Conference on Decision and Control, Honolulu, Haway, 1990.

[23] A. Siddiqi, Identification of the harmonic transfer functions of a helicopter rotor, Ph.D. thesis, Massachusetts Institute of Technology (2001).

[24] S. J. Shin, C. E. Cesnik, S. R. Hall, System identification technique for active helicopter rotors, Journal of Intelligent Material Systems and Structures 16 (11-12) (2005) 1025–1038.

[25] R. Gori, F. Pausilli, M. D. Pavel, G. M, State-space rotor aeroelastic modeling for real-time helicopter flight simulation, Advanced Material Research 1016 (2014) 451–459.

[26] M. Gennaretti, G. Bernardini, J. Serafini, G. Romani, Rotorcraft comprehensive code assessment for blade-vortex interaction conditions, Aerospace Science and Technology 80 (2018) 231–246.